



HAL
open science

Thermo-chemo-mechanical behavior of alkali-activated slag materials - Focus on early-age

F. Rifai, A. Darquennes, F. Benboudjema, B. Muzeau, L. Stefan

► **To cite this version:**

F. Rifai, A. Darquennes, F. Benboudjema, B. Muzeau, L. Stefan. Thermo-chemo-mechanical behavior of alkali-activated slag materials - Focus on early-age. 2nd International RILEM/COST Conference on Early Age Cracking and Serviceability in Cement-based Materials and Structures - EAC2, Sep 2017, Brussels, Belgium. hal-02417342

HAL Id: hal-02417342

<https://hal.science/hal-02417342>

Submitted on 18 Dec 2019

HAL is a multi-disciplinary open access archive for the deposit and dissemination of scientific research documents, whether they are published or not. The documents may come from teaching and research institutions in France or abroad, or from public or private research centers.

L'archive ouverte pluridisciplinaire **HAL**, est destinée au dépôt et à la diffusion de documents scientifiques de niveau recherche, publiés ou non, émanant des établissements d'enseignement et de recherche français ou étrangers, des laboratoires publics ou privés.

Thermo-chemo-mechanical behavior of alkali-activated slag materials Focus on early-age

Farah Rifai ^{*a,b}, Aveline Darquennes^b, Farid Benboudjema^b, Benoist Muzeau^a, Lavinia Stefan^c

^a Den-Service d'Etude du Comportement des Radionucléides (SECR) CEA, Université Paris-Saclay
F-91191, Gif-sur-Yvette, France

^b LMT Cachan – ENS Cachan – Paris-Saclay University, Cachan, France

^c AREVA NC, DM2D, Technical Direction, La Défense, France

ABSTRACT

This study addresses the development of a modelling approach predicting the behavior of waste packages made with an alkali activated slag mortar. Durability of such structures is studied regarding the restriction of hydraulic binder's strains by the rigid inclusions and the wasteforms' container. The current work focuses on early-age behavior. First, the evolution of material's mechanical properties and delayed strains (autogenous shrinkage and basic creep) are determined experimentally. Results show that equivalent time approach should be used for simulations to address correctly the time-dependent evolution of mechanical parameters, rather than an approach based on hydration degree (determined by calorimetry). For basic creep, the use of an aging dashpot seems to be sufficient. Then, finite element calculations at meso-scale are performed to determine homogenized properties of binder/waste assembly. Results are used for macro-scale simulations.

Keywords: alkali-activated slag, hydration, shrinkage, creep, durability

1. INTRODUCTION

Ground Granulated Blast Furnace Slag (GGBFS) is a by-product of steel industry that has long been used as cement blending material. The high amount of CO₂ emissions resulting from the fabrication of ordinary Portland cement has encouraged the adoption of this material as a hydraulic binder¹⁻². Additionally, alkali-activated slag binders have shown advantages as an alternative for Portland cement in some specific applications¹⁻³⁻⁴⁻⁵.

This work addresses the thermo-chemo-mechanical behavior of a sodium hydroxide activated slag mortar presently under study as an immobilization matrix for the conditioning of nuclear waste in France. The durability of waste packages is guaranteed for several decades, thus evaluating the damage risk is of great importance. The present work is concerned by the restriction of binder's delayed strains. Hence, a modelling approach based on an experimental campaign is being developed. In this paper, the experimental and numerical work undertaken in order to describe the evolution of the autogenous shrinkage and the basic creep of the hydraulic binder is discussed. Additionally, the homogenization method used to take into account the presence of inclusions is developed. At the end, the model is tested at macro-scale level with simulations undertaken on a massive structure with arbitrary parameters.

2. EXPERIMENTAL WORK AND MODELING

The analysed binder composition is activated by a sodium hydroxide solution. An initial water to binder ratio (w/b) of 0.5 is used as well as a sand to binder ratio (s/b) equal to 2. All the experiments were conducted on specimens kept in autogenous conditions (protected by plastic film and aluminium sheets after demoulding at the age of 24 hours in order to inhibit moisture transfer) and placed in a controlled room (25 ± 1°C and 35 ± 5% RH).

2.1 Autogenous shrinkage strains

The autogenous shrinkage strains of alkali-activated slag mortar were continuously measured on three different 4x4x16 cm specimens using linear variable differential transformer (LVDT) sensors. Results are illustrated in figures 1 and 2.

* farah.rifai@cea.fr; phone +33 (0)1 69 08 98 53

Two different modelling approaches are tested. The first one is the classical approach used for hydraulic binders. The degree of advancement of hydration reactions is calculated based on the affinity model calculated from semi-adiabatic calorimetric measurements as shown in a previous work⁶⁻⁷⁻⁸. A linear dependency of autogenous shrinkage strains $\varepsilon^{au}(t)$ is usually valid⁸⁻⁹ according to equations 1, 2 and 3.

$$\xi(t) = A(\xi) \exp\left(-\frac{E_a}{RT}\right) \quad (1) \quad \bar{\xi}(t) = \frac{\xi(t) - \xi_0}{\xi_\infty - \xi_0} \quad (2) \quad \varepsilon^{au}(t) = -K \times \bar{\xi}(t) \quad (3)$$

Where ξ is the degree of advancement of hydration reaction [-], E_a is the activation energy [J.mol⁻¹], R the universal gas constant [8.3144621 J.mol⁻¹.K⁻¹], $A(\xi)$ is the chemical affinity [s⁻¹], ξ_∞ the ultimate degree (taken equal to 1), ξ_0 the percolation threshold based on Vicat needle test [0.02 -] and K a constant. The chemical affinity is modelled using a polynomial function of degree six.

Second, the mathematical function used in EC2^a for the description of mechanical properties development, function of the equivalent time is tested. The setting time is introduced to account for the percolation threshold as shown in the following equations:

$$t_e(t, T) = \int_0^t \exp\left[-\frac{E_a}{R}\left(\frac{1}{T} - \frac{1}{T_{ref}}\right)\right] dt \quad (4) \quad \beta_c(t_e) = \exp\left[s\left(1 - \sqrt{\frac{28}{(t_e - t_0)_+}}\right)\right] \quad (5) \quad \varepsilon^{au}(te) = \varepsilon^{au}_{28} \times (\beta_c)^{n_{\varepsilon^{au}}} \quad (6)$$

Where t_e is the equivalent time [days], T_{ref} the reference temperature taken equal to 25°C and t_0 the setting time [days].

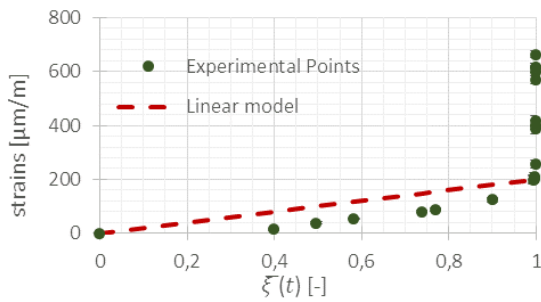


Figure 1: Comparison between experimental and predicted (hydration reactions' advancement degree approach) autogenous shrinkage strains

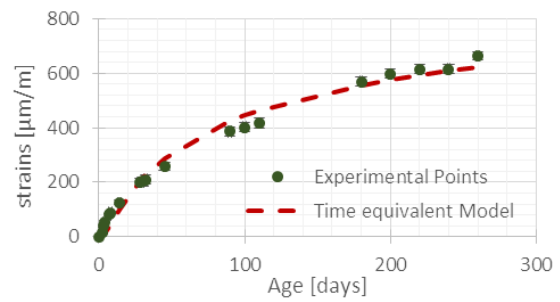


Figure 2: Comparison between experimental and predicted (equivalent time approach) autogenous shrinkage strains

The experimental results of Figure 1 show that the model widely used for classical cementitious materials' shrinkage is not valid for the studied binder. In fact, at the long term, shrinkage strains continue to increase whereas the advancement degree based on calorimetric test reaches one. The time equivalent model plotted in Figure 2 seems to describe correctly the behaviour of the alkali-activated mortar. These strains are very important with a significant evolution even after 200 days of measurements. Note that duplicate specimens were used for mass loss measurement to check that the autogenous cure conditions remain valid for the whole test duration.

In order to check if this problem originates from the affinity function definition determined based on semi-adiabatic calorimetric tests, a validation test is conducted. An isothermal micro-calorimetric test is performed using a "Tam Air Isothermal Calorimeter" with a precision of 20 μW at 22°C. Numerical simulation results and experimental data are compared in terms of degree of advancement of hydration reactions based on 720 hours of heat measurements.

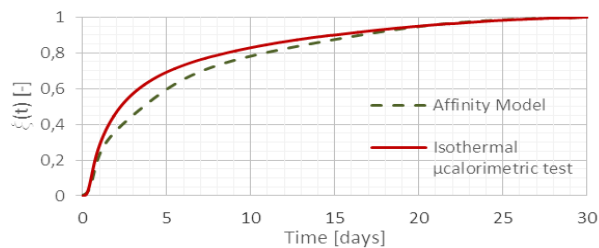


Figure 3: Hydration reactions' advancement degree determined according to isothermal micro-calorimetry heat measurements and affinity model's thermo-chemical simulations

^a EC2. (1992). Eurocode 2 - part1. Design of concrete structures.

The comparison between both evolutions illustrated in Figure 3 shows that the affinity model is capable of predicting the advancement of hydration reactions. Therefore, the divergence of shrinkage experimental results from the linear model could be related to the difference in hydration mechanisms between alkali-activated slag mortar and classical cementitious materials.

2.2 Basic creep

Taking into account the visco-elastic behavior of hydraulic binders in numerical simulation is of great importance. In fact, when material's basic creep is not included, the generated stress is overestimated in calculations. Very little interest was shown in the literature regarding this type of delayed strains for alkali-activated binders¹⁰. In the current study, the basic creep of the alkali-activated mortar is determined under compressive stress. 7x7x28 cm specimens kept in autogenous conditions are used and tests are conducted in the same controlled room. Two samples are loaded, at the age of 7 and 28 days, at 30% of their compressive strength at the respective ages. A dashpot rheological model¹¹ with ageing viscosity is used according to the following equations:

$$\varepsilon^{bc}(t) = \frac{\sigma_0}{\eta(t_e)} \quad (7) \quad \eta(t_e, t') = \eta_{28} \times (\beta_c(t_e))^{n_\eta} \times t_e \quad (8)$$

Where ε^{bc} is the basic creep strains' tensor [$\mu\text{m/m}$], σ_0 the applied compressive stress [Pa] and η the aging viscosity parameter [Pa.s].

Experimental and modeling results are compared in the following figure:

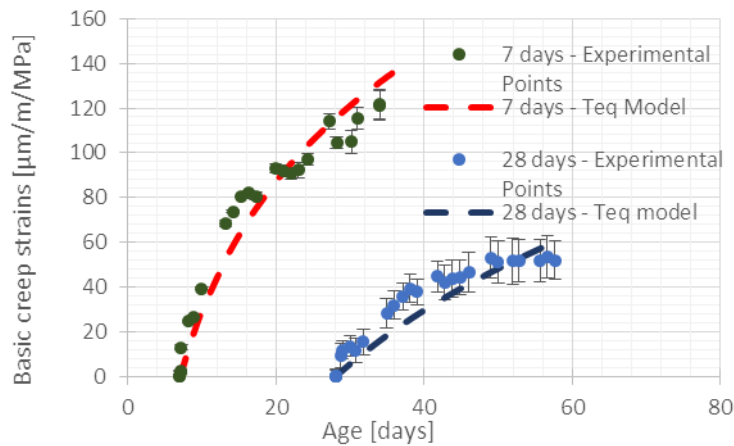


Figure 4: Time evolution of basic creep strains of alkali-activated slag mortar under compressive loading starting at the ages of 7 and 28 days at 30% of compressive strength

The alkali-activated mortar has high creep capacity (comparing to ordinary cementitious mortar with same w/b and s/b ratios). This could be explained, at long term, by the higher amount of C-S-H present in the alkali-activated slag systems¹². In fact, the long term part of basic creep is usually explained by the mechanical sliding of C-S-H¹³. The proposed numerical model is adequate for the description of this behavior and thus for conducting numerical simulations able to reproduce the significant stress relaxation in structures made of alkali-activated mortar.

3. FINITE ELEMENT HOMOGENISATION

The encapsulated rigid wastes restrain the shrinkage of the alkali-activated matrix. This results in tensile stress generation in the binder. Multi-scale modelling approach is thus relevant in this case of study. Simulations at meso-scale provide upscaled material properties (thermal conductivity, Young modulus etc...) but also generated stresses by self-restraints (inclusion/binder). The first type of elastic calculations, undertaken by means of finite element simulations in order to determine the global autogenous shrinkage and the Young modulus evolution of the representative elementary cell (binder + inclusions), is discussed here-after.

3.1 Equivalent autogenous shrinkage evolution

The mesh illustrated in Figure 5 is used for calculations conducted in 2D. Dimensions of matrix (binder) and inclusions elements are determined with respect to wastes' volume fraction (50% in the example shown here). Mechanical properties of the binder are also expressed in function of equivalent age⁶.

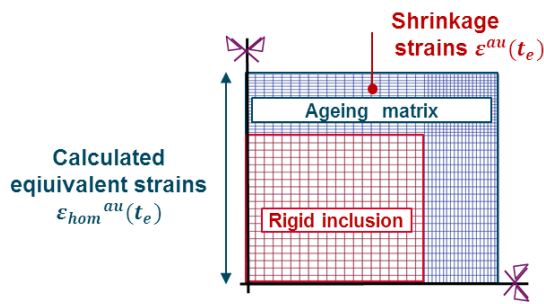


Figure 5 : Schematic of the representative elementary volume and symmetry conditions used for FE homogenization calculations of autogenous shrinkage strains

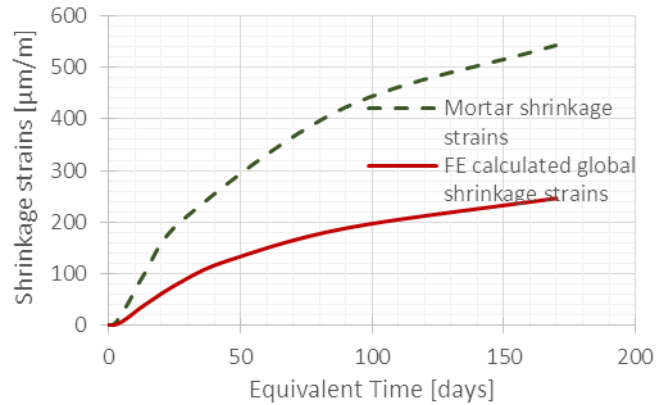


Figure 6: Finite element calculations of homogenized autogenous shrinkage expressed in function of equivalent time

The mechanical properties of the inclusions are fixed (Young modulus of 30 GPa – Poisson ratio of 0.35 here). Global (homogenized) autogenous strains can be thus calculated and expressed in terms of equivalent time. Results are illustrated in Figure 6. The restriction of binder's strains is reproduced. A decreasing reduction from 67% (at day 3) to 55% (at day 180) of autogenous strains is obtained for 50 % (in volume) of inclusion.

3.2 Equivalent mechanical properties

In order to calculate the homogenized mechanical properties, the same mesh described in the previous section is used. For instance, the simulated mechanical behavior of the cell to an imposed known displacement gives the global Young modulus as shown in Figure 7. Once again, mechanical properties of binder's elements are expressed in function of equivalent time while the inclusions has fixed Young modulus and Poisson ratio.

Results are illustrated in Figure 8. The time-evolution of calculated Young modulus is compared to the one that could be evaluated with the Mori-Tanaka homogenization scheme ¹⁴.

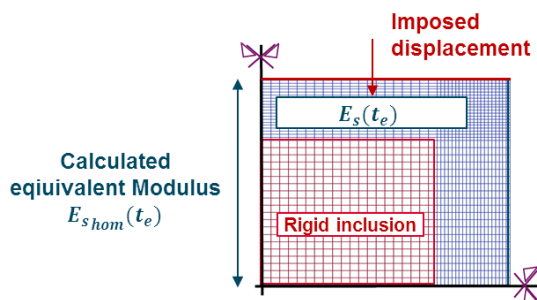


Figure 7: Schematic of the representative elementary volume and symmetry conditions used for FE homogenization calculations of Young modulus evolution

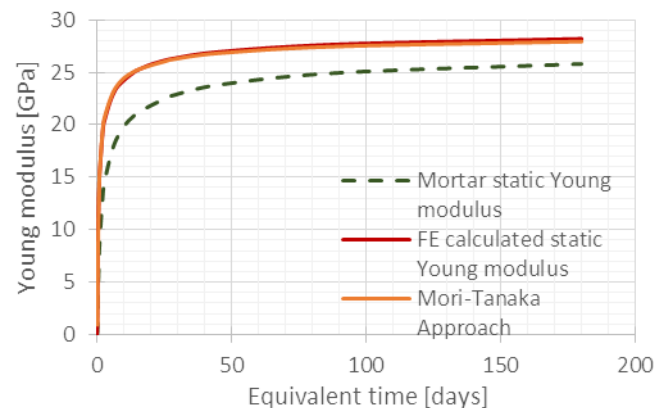


Figure 8: Finite element calculations of homogenized Young modulus expressed in function of Equivalent time

The calculated Young modulus shows good accordance with the classical Mori-Tanaka scheme. An increase in rigidity of 40% at day 3 to 10% at day 180 is obtained for 50 % of inclusion. The effect of rigid inclusions decreases with the evolution of the binder's Young modulus approaching the inclusions' one.

4. MACRO-SCALE CALCULATIONS AT EARLY-AGE

In this section, the thermo-chemo-mechanical model developed is tested on a massive structure having the same dimensions of the waste packages. Basic creep strains are not yet taken into account. Fraction volume of inclusions is

taken equal to 0.5. These parameters are not identical to the real waste package. They are arbitrarily chosen to test the model.

4.1 Mechanical analysis

A damage approach is used to describe cracking that occurs mainly in tension at early-age (due to the restrain of strains) based on Mazars model ¹⁵ with some modifications developed in a previous work ⁶. The relationship between apparent stresses σ , effective stresses $\bar{\sigma}$, damage D , elastic stiffness tensor E , elastic strains ε_{el} reads equation 9:

$$\sigma = (1 - D)\bar{\sigma} \quad (9) \quad \dot{\bar{\sigma}} = E \dot{\varepsilon}_{el} = E (\dot{\varepsilon} - \dot{\varepsilon}_{hom}^{au} - \dot{\varepsilon}_{hom}^{th}) \quad (10)$$

Elastic strains tensor ε_{el} is expressed in terms of total strains ε , autogenous strains ε_{hom}^{au} and thermal strains ε_{hom}^{th} tensors as shown in equation 10. The latter tensor is calculated as indicated mentioned in a previous work ^[6], taking into account the effect of inclusion on the thermal properties of the assembly (binder + inclusion). It will not be detailed here.

The damage criterion given f takes into account the calculated homogenized mechanical properties:

$$f = \hat{\varepsilon} - \kappa_0 \quad (11) \quad \kappa_0 = \frac{f_{t_{hom}}(t_e)}{E_{s_{hom}}(t_e)} \quad (12)$$

Where κ_0 is the tensile strain threshold computed from the evolution of the homogenized mechanical properties $f_{t_{hom}}(t_e)$ and $E_{s_{hom}}(t_e)$.

4.2 Results

Computation results, obtained by adopting the mesh and the boundary conditions illustrated in Figure 9, are presented in the stress map at 28 days of Figure 10. An axisymmetric model with regular 4-node element mesh is used. The evolution of stress in the specific points indicated on the mesh (P1 at the center where max of heat occurs and P2 intermediate point) are represented in Figure 11.

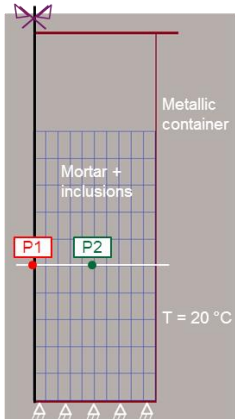


Figure 9 : Calculation mesh and boundary conditions

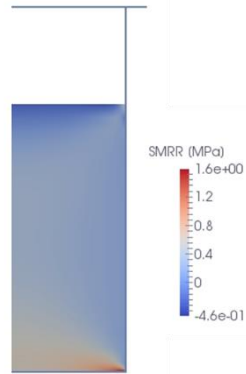


Figure 10: Radial stress map in simulated structure at 28 days

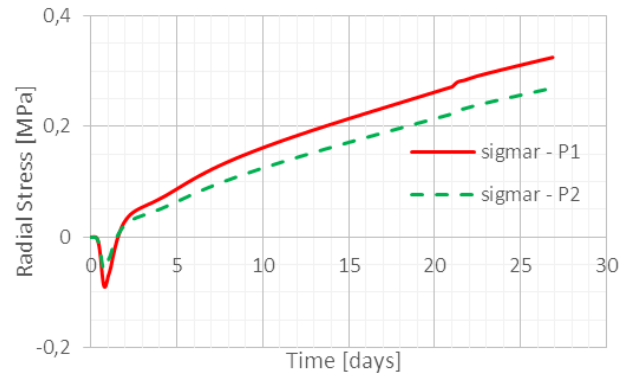


Figure 11: Internal radial stress evolution in simulated structure at points P1 and P2

The results show the effect of the thermal gradient at early-ages: center expansion due to the hydration reactions' heat release is restricted by the surface subjected to a lower temperature. This effect leads to compressive stress generation at the center of the massive structure. These stresses are higher at the center of the structure than at the intermediate point that is closer to the outer surface. After-on, the tensile stresses generated from the restriction of delayed strains appear. Analysis of the stress distribution in the simulated package show that no damage occur during the first 28 days and therefore no cracking risks are predicted.

5. CONCLUSIONS

The study presented here discussed first the experimental investigation of alkali-activated slag mortar delayed behavior. A finite element based method is then used for the simulation. Homogenized properties are calculated at meso-scale to describe the behavior of the matrix/inclusion assembly. Meso-scale properties are afterwards implemented in macro-scale calculations. Damage analysis with evolutionary mechanical properties expressed in terms of equivalent time model is applied. The following conclusions can be drawn:

- Autogenous shrinkage strains of alkali activated slag binders are significantly high and do not show a stabilization even after 250 days. The classical thermo-chemo mechanical modelling used for OPC binders (based on quasi-adiabatic or isothermal calorimetry tests for parameters identification) is unsuitable for this type of binders. However, equivalent time modelling seemed to be adequate. Additional data will be collected on the long term to check the capability of this model to predict long term delayed behavior,
- Basic creep strains of the material are shown to be important at 7 and 28 days. The increase in creep capacity with the advancement of hydration (with time) is observed for the alkali-activated slag as for OPC. Furthermore, the dashpot rheological model expressed in terms of equivalent time is valid for numerical simulation,
- Finite element meso-scale calculations can be used to determine the effect of rigid inclusions on the macro-scale behavior of binder/waste assembly. Meso-scale results show the contribution of rigid waste in the reduction of the binder's delayed strains and the increase of its rigidity,
- Modified damage model based on Mazars' model is used to take into account the evolution of mechanical properties in function of equivalent time.

ACKNOWLEDGEMENTS

The authors would like to extend their appreciation and gratitude for the financial support to the project provided by CEA and "New Areva".

REFERENCES

1. Scrivener, L., Kirkpatrick, J.: Innovation in use and research on cementitious material. *Cement and concrete research* 38, 128-136 (2008)
2. Davidovits, J. : *Ciments géopolymères. Techniques de l'ingénieur* (2014)
3. Provis, J. and van Deventer, J.: Alkali activated materials. (Eds) State of the art report. RILEM TC224-AAM (2014)
4. Deja, J.: Immobilization of Cr⁶⁺, Cd²⁺, Zn²⁺ and Pb²⁺ in alkali-activated slag binders. *Cement and concrete research* 32, 1971-1979 (2002)
5. Shi, C. and Fernandez-Jimenez, A.: Stabilization/solidification of hazardous and radioactive wastes with alkali-activated cements. *Journal of hazardous materials B137*, 1656-1663 (2006)
6. Rifai, F., Darquennes, A., Benboudjema, F., Muzeau, B., & Stefan, L.: Study of shrinkage restraint effects at early-age in alkali-activated slag mortars. 9th international conference on fracture mechanics of concrete and concrete structures FraMCoS-9. Berkeley. doi:DOI 10.21012/FC9.240 (2016)
7. Lackner, R. and Mang, H.A.: Chemo-plastic material model for the simulation of early age cracking: From the constitutive law to numerical analyses of massive concrete structures. *Cement and concrete composites* 26, 551-562 (2004)
8. Ulm, F.J. and Coussy, O.: Coupling in early-age concrete: From material modelling to structural design. *International Journal of Solids and Structures* 35, 4295-4311 (1998)
9. Benboudjema, F., & Torrenti, J.-M.: Early-age behaviour of concrete nuclear containments. *Nuclear Engineering and Design* 238(10), 2495-2506 (2008)
10. Collins, F. G., & Sanjayan, J. G.: Workability and mechanical properties of alkali activated slag concrete. *Cement and Concrete Research* 29(3), 455-458 (1999)
11. Hilaire, A. : Etude des déformations différées des bétons en compression et en traction, du jeune au long terme : application aux enceintes de confinement. PhD Dissertation. Ecole Normale Supérieure de Cachan, France (2014)
12. Gruskovnjak, A., Lothenbach, B., Holzer, L., Figi, R and Winnefeld, F.: Hydration of alkali-activated slag: comparison with ordinary Portland cement. *Advances in Cement Research* 18(3), 119-128 (2006)
13. Ulm, F.-J. et Acker, P.: Le point sur le fluage et la recouvrance des bétons. Technical report. Bulletin des Laboratoires des Ponts et Chaussées. (Spécial XX):73–82 (1998)
14. Smilauer, V., Bittnar, Z.: Microstructure – based micromechanical prediction of elastic properties in hydrating cement paste. *Cement and Concrete Research* 36(9), 1708-1718 (2006)
15. Mazars, J.: A description of micro and macroscale damage of concrete structures. *Engineering Fracture Mechanics* 25, 729-737 (1986)